Vehicle System Dynamics: International Journal of Vehicle Mechanics and Mobility
Publication details, including instructions for authors and subscription information:
http://www.tandfonline.com/loi/nvsd20

A Mathematical Model for Driver Steering Control, with Design, Tuning and Performance Results

R.S. Sharp , D. Casanova & P. Symonds

Published online: 09 Aug 2010.

To cite this article: R.S. Sharp , D. Casanova & P. Symonds (2000) A Mathematical Model for Driver Steering Control, with Design, Tuning and Performance Results, Vehicle System Dynamics: International Journal of Vehicle Mechanics and Mobility, 33:5, 289-326

To link to this article: http://dx.doi.org/10.1076/0042-3114(200005)33:5;1-Q;FT289

Vehicle System Dynamics, 33 (2000), pp. 289–326 0042-3114/00/3305-289$15.00

A Mathematical Model for Driver Steering Control, with Design, Tuning and Performance Results

R. S. SHARP*, D. CASANOVA* and P. SYMONDS†

SUMMARY

A mathematical model for the steering control of an automobile is described. The structure of the model derives from linear optimal discrete time preview control theory but it is non-linear. Its parameter values are obtained by heuristic methods, using insight gained from the linear optimal control theory. The driver model is joined to a vehicle dynamics model and the path tracking performance is demonstrated, using moderate manoeuvring and racing speeds. The model is shown to be capable of excellent path following and to be robust against changes in the vehicle dynamics. Application to the simulation of manoeuvres specified by an ideal vehicle path and further development of the model to formalise the derivation of its parameter values and to put it to other uses are discussed.

1. INTRODUCTION

Modelling and simulation are integral components of contemporary vehicle dynamics. In order to predict quality of performance of a vehicle in its design stage or to trouble shoot problems appearing with actual vehicles, simulations of a large number of different manoeuvres will be necessary, from time to time. Some manoeuvres which are routinely used for subjective assessment of handling qualities by drivers are specified by the control inputs, while others involve path following. An example of the latter is the lane change manoeuvre, in which the driver's steering input is whatever is necessary, in view of the vehicle being tested, to follow the prescribed path. In the theoretical world too, it is required to calculate vehicle responses to specified control inputs, on the one hand, and to simulate a path following event, on the other. A special class of manoeuvres, which currently receives much attention, is the traversing of a circuit of known geometry by a racing car.

The first of these is straightforward but the second demands something more than

* School of Mechanical Engineering, Cranfield University, Bedford MK43 0AL

† Benetton Formula Ltd, Whiteways Technical Centre, Enstone, Chipping Norton, Oxford OX7 4EE

just a vehicle simulation model. To work out the control inputs to successfully follow a path, either the inverse dynamics problem has to be solved [2, 3] or a driver representation needs to be added to the vehicle dynamics model. Several such models have been described in the literature and a short review of the main ideas used follows.

The earliest driver model of note was the 'cross-over' model [13]. The cross-over model depends on representing driving as a small perturbation regulation task. Experimental testing of man-machine systems has shown that people will adopt a describing function: $Y_p = K_p e^{-j\omega\tau}(1 + T_L j\omega) / \{(1 + T_I j\omega)(1 + T_N j\omega)\}$ in a regulation task, with the time delay τ representing a reaction time delay, T_N representing muscular actuation delays and T_L and T_I representing lead/lag time constants associated with data processing. K_p is a gain chosen by the person, to ensure stability of the closed loop system, preferably over a broad frequency range. The open loop response function magnitude $|Y_p Y_c|$ will have a -20dB/decade slope in the frequency region surrounding the 'cross-over' frequency (see below) and $|Y_p Y_c|$ >>1 at low frequencies. Simplified, this implies that the person will adapt a describing function Y_p, in recognition of the machine response function Y_c, such that $Y_p Y_c = \omega_c e^{-j\omega T} / j\omega$ in the region of the cross-over frequency. This frequency turns out to be the gain ω_c, which is the frequency at which the open loop system has unity gain. The closed loop system bandwidth rises with ω_c, so that those machine characteristics which encourage large ω_c make for a good performing system. Highest ω_c comes from the need for driver low frequency lag. If low frequency lead is necessary, it causes low cross-over frequency and poor closed loop system performance.

The cross-over model nicely represents the adaptation of a person to a machine and allows one to judge between machines. However, its foundation is in regulatory tasks, the main one of which in driving is travelling in a straight line under cross-wind disturbance. Attempts to extend its domain to cover more general driving appear contrived and only marginally effective [5]. Since the main concern here is with path following with path preview, the cross-over model will not be discussed further.

Driver models based on preview of the road ahead were reviewed by [6]. As indicated there, substantial progress in driver modelling, but still in a linear world, was made by [8]. He represented the driver as an optimal preview controller, constructing a path error functional by previewing the road over a known preview distance, and minimising a weighted integral of squares of differences between the previewed path points and the corresponding estimated lateral positions of the vehicle over the preview distance. The main weakness of the theory, as pointed out by Guo and Guan, is the need to presume a constant control input over the preview interval in

order to estimate the vehicle position. Notwithstanding this presumption, the theory, in single preview point form, was shown to more or less subsume the cross-over model for a regulation task and to be quite capable in respect of path following control. In this case, integrals were calculated approximately by discrete computations allowing 10 equally spaced preview points over the preview interval. Many detailed developments from this starting point are described by the reviewers, concentrating on the relatively elementary single preview point cases. This particular feature is considered unrealistic and unsatisfactory, since it is clear that if the preview point is a long way in front of the vehicle, it will be inappropriate to act on the preview information at the time of its acquisition and the information has gone by the time it is useful. On the other hand, if the preview point is very close to the vehicle, control will necessarily be very poor. It is always the case that with single point preview models, the first concern in choosing parameter values is to set a preview distance which is reasonable [7]. One cannot imagine a real driver using single-point preview.

In parallel with work on driver steering models, optimal linear preview control theory has been applied extensively to active vehicle suspensions, an overview of which has been given by [11]. Both continuous time and discrete time approaches have been followed, the latter leading to rather simpler interpretations. It has been established that optimal linear preview control involves diminishing returns; for any task, there is an amount of preview beyond which further preview is of no value to the controller. If such further preview were available, the controller would take no notice of it. In discrete time, optimal use of the preview data involves forming a weighted sum of the preview error samples and using the sum for control. In the complete optimal scheme, this sum is combined with a corresponding sum of weighted state feedback terms to give the required control. If the preview is foreshortened, the optimal gains are unaltered. What happens to the optimal control is that it is just the remainder from the infinite preview case, with the lost preview information simply missing. Finally, the gain sequence associated with the preview error samples reflects the dynamics of the controlled plant, indicating the use of the preview control to motivate the system by operating preferentially on its eigenmodes. Thus, if the plant has a lightly damped mode, and the control bandwidth is sufficient to excite that mode, the optimal preview control gain sequence will show the oscillatory pattern of the eigenmode. On the other hand, if the plant is very well damped, the gain sequence will appear more like an exponential convergence on zero gain for large preview distance.

If this set of ideas from suspension control is taken across into the world of driver modelling, the following picture emerges. While the vehicle is operating in its linear region, the linear discrete time optimal preview control theory applies directly. It indicates that the driver will acquire path preview information by looking ahead of the vehicle, forming lateral position error estimates by comparison of the path ahead with points along an imaginary optical lever projecting forwards from the vehicle, see below. The driver will also have state error information from the relation between the

present position and that desired (perfectly on the path). These error estimates will be weighted and summed, the preview weighting values reflecting the vehicle lateral dynamics, to some extent. The state feedback gains are those which belong to the non-preview case. The control scheme is illustrated in Figure 1.

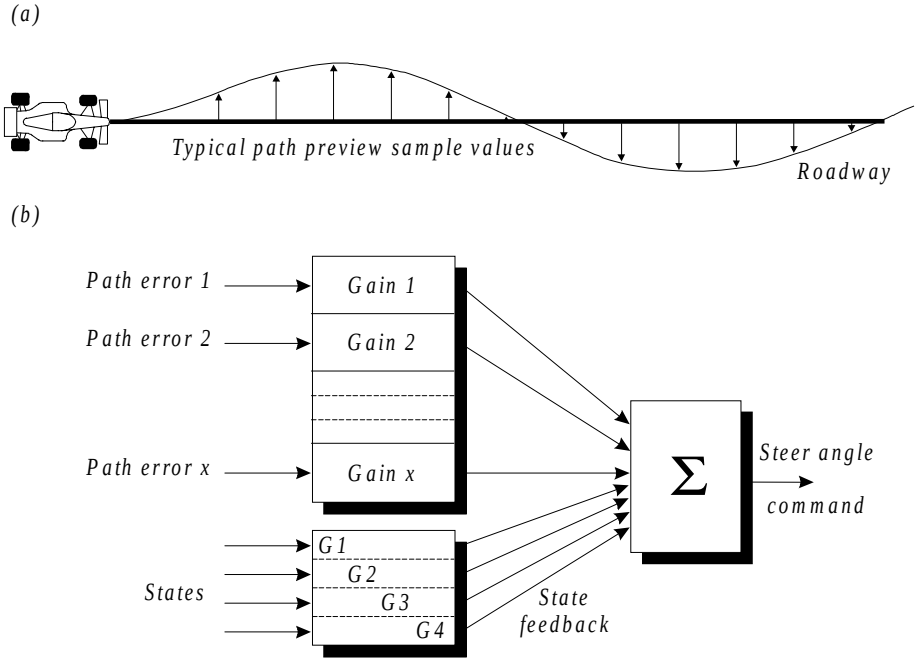

Fig. 1. Notional structure of optimal linear preview driving controller

In vigorous manoeuvring, tyre forces saturate and imply non-linear vehicle behaviour. To deal with this case, it can be observed that the structure of the control scheme in Figure 1 is that of a linear neural network. It is apparent that the saturating non-linearity of the real vehicle can be accommodated by the replacement of the linear network by a non-linear one. It can be anticipated that the optimal linear gains will provide a starting point for the calculation of good network parameters, refinement coming from a learning process[*].

In more recent work, MacAdam and Johnson [9] have shown interest in neural network structures for driving control. They argue for more than one preview point, using three in fact, and they attach value to the possibility of combining preview

[*] Since the paper was first written, a Masters student has obtained a linear optimal discrete time solution to the quadratic path error minimisation problems for a yaw-sideslip car. The form of the solution aligns well with that anticipated. It is intended to offer this work for publication when it is complete.

sample values by differencing (say) to obtain implied path orientation data. They also value time-delayed versions of the path preview samples and feed some time-delayed observations into their control network alongside the three current preview sample values. The association made by the present authors between linear optimal discrete time preview suspension control and driving suggests a different interpretation of the value of this time-delayed data, since the optimal suspension controller does not calculate differences between preview samples or combine them in other ways. Neither does it do anything equivalent to using the path preview samples to compute the future path of the vehicle, based on some model of the vehicle dynamics. The structure of the optimal linear controller suggests that it is not necessary to perform these operations on the preview data, provided that the preview points are sufficiently closely spaced.

The paper goes on to apply the above framework to setting up a particular driver model, which will deal with the non-linear vehicle operating regime. In its current form, the model parameters are derived in an ad hoc fashion, based on intuition and not on any formal optimisation scheme. Parameter values are set and the thinking behind their derivation is exposed. Saturation properties are introduced into the controller, to match the saturation properties of the vehicle tyres, to a certain extent. The application of the model to path following tasks, associated with moderate manoeuvring and with circuit racing at the limits of possible performance, is described. The driver model is linked to a non-linear vehicle dynamics model, so that the combination can attempt to follow a prescribed path. Good path following capabilities and robustness of the controller are demonstrated. General rules for setting the controller parameters and performance issues are considered. The paper concludes with a discussion of further work necessary to formalise the processes by which good model parameters can be derived and to reflect on future applications of advanced driver models.

2. THE PATH FOLLOWING PROBLEM

2.1. The control task

The steering control model task is to monitor the ideal path ahead of the vehicle and to derive from the observations the steering wheel displacement which will yield effective path following. The vehicle longitudinal motion will be separately specified. At the simplest level, the vehicle forward velocity may be set equal to a constant value. Alternatively, either the vehicle longitudinal control or the longitudinal velocity may be given as a function of the position along the intended path. In this work the last approach, which involves the solution of the vehicle longitudinal inverse dynamics, is considered. It is important to notice that the lateral and longitudinal vehicle controls are treated as being completely uncoupled. As a result,

the intended manoeuvre may be infeasible, e.g., the longitudinal velocity or the vehicle thrust may be too high for a certain cornering radius. The simulation programme must be able to handle these exceptional conditions, and its capability in this respect will be demonstrated.

2.2. Ideal path description

The parameters used to describe the ideal path are those illustrated in Figure 2; the path curvature k_t, the tangent angle ψ_t, and the co-ordinates x_t and y_t measured from the axis reference system fixed in space. These parameters are taken as functions of the path length co-ordinate s. Road camber and elevation are not considered, but the extension would be straightforward if they were to be included in the vehicle modelling. Although the way that these data are organised and loaded in the simulation is arbitrary to a great extent, in the description of the driver model and its implementation we shall refer to a matrix of path information with the following structure:

$$\mathbf{T_{RJ}} = \begin{bmatrix} \mathbf{s} & \mathbf{k_t} & \boldsymbol{\psi}_\mathbf{t} & \mathbf{x_t} & \mathbf{y_t} \end{bmatrix}$$

The first column specifies the distance from a chosen origin of a set of points along the ideal path, e.g., every five meters; the other columns contain the corresponding values of the path parameters.

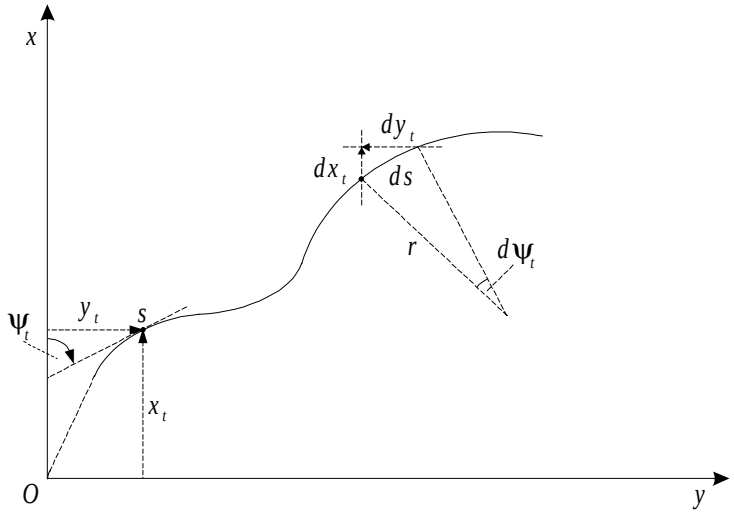

Fig. 2. Ideal path description

The method to generate a set of path data which is favoured here, consists of starting from a known curvature function of the path distance and integrating it twice to obtain the other parameters, according to the following relations (see Fig. 2):

$$\psi_t(s) = \int_0^S k_t(s)ds \tag{1}$$

$$x_t(s) = \int_0^S \cos\left(\psi_t(s)\right)ds \tag{2}$$

$$y_t(s) = \int_0^S \sin\left(\psi_t(s)\right)ds \tag{3}$$

The curvature of the ideal path may just be invented, e.g., to create lane change manoeuvres, or it may be calculated from the vehicle longitudinal velocity V_{vx} and lateral acceleration a_{vy} which are measured on board a race car, using the following kinematic relationship:

$$k_t(s) = \frac{1}{r(s)} \cong -\frac{a_{vy}(s)}{V_{vx}^2(s)} \tag{4}$$

This allows one to determine an estimate of a race car trajectory round a circuit, as will be shown in the results at the end.

3. VEHICLE MODEL OUTLINE

3.1. Chassis description

The vehicle is represented with a five degrees of freedom model. The chassis is described as a rigid body with three degrees of freedom, the yaw angle and the lateral and longitudinal displacements. The wheels are rigidly attached to the body, allowing only rotation relative to the vehicle chassis about their spin axes. Furthermore, the wheels on the same axle are constrained to have the same angular velocity. Therefore only two extra degrees of freedom are added. Although the suspensions are not included in the modelling, the roll axis position, the roll stiffness distribution, the mass centre height and the track width are parameters taken into account in order to allow an approximate evaluation of the lateral load transfer corresponding to a lateral acceleration of the mass centre.

3.2. Aerodynamic forces

A simple representation of the aerodynamic forces is employed by assuming constant drag and lift coefficients. The aerodynamic drag is applied at the height of the vehicle centre of gravity. The centre of application of the aerodynamic lift is the same for all speeds and is determined by specifying the down force distribution between the front and the rear axles.

3.3. Tyre forces

The tyre lateral and longitudinal forces are introduced using the Magic Formula Tyre Model which features the use of weighting functions to account for combined slip conditions [10]. The tyre slip quantities are evaluated with the assumption of small angles and they are referred to the centre of the front and rear axles, as for a bicycle model. Static wheel camber angle settings are accounted for. Figure 3 shows the tyre forces at pure slip for a range of vertical loads representative of the vehicle working conditions at different velocities.

3.4. Wheel vertical loads

The wheel vertical loads are evaluated accounting for the vehicle static weight distribution, the aerodynamic down-force distribution and the longitudinal and lateral load transfers when the vehicle is driving, braking and cornering. The load transfers are estimated on the basis of a steady state analysis considering the vehicle longitudinal and lateral accelerations.

3.5. Vehicle lateral and longitudinal controls

The lateral control variable is the steer angle applied to the front wheels. The geometry of the steering system is not included in the modelling and the steer angle is thought to be the same for the left hand side wheel and the right hand side wheel. The longitudinal control variable is the driving or braking torque, the former applied to the rear axle only, the latter applied to both front and rear axles according to a constant distribution scheme. In order to obtain results that are comparable to data measured on a real race car, the vehicle model includes a number of parameters of the drive train:

- the gear ratios, which are selected upon the vehicle velocity;
- the engine moment of inertia, which has a significant contribution when the vehicle is accelerating in low gears;
- the engine braking torque at closed throttle position, which may alter the braking force distribution significantly.

The engine driving torque characteristic is not considered in the modelling, it being assumed that it is always sufficient to maintain the intended forward motion. After the simulation, from the value of the longitudinal control and the gear ratio, the throttle position may be reconstructed using the map of the engine torque output, allowing one to verify the above assumption.

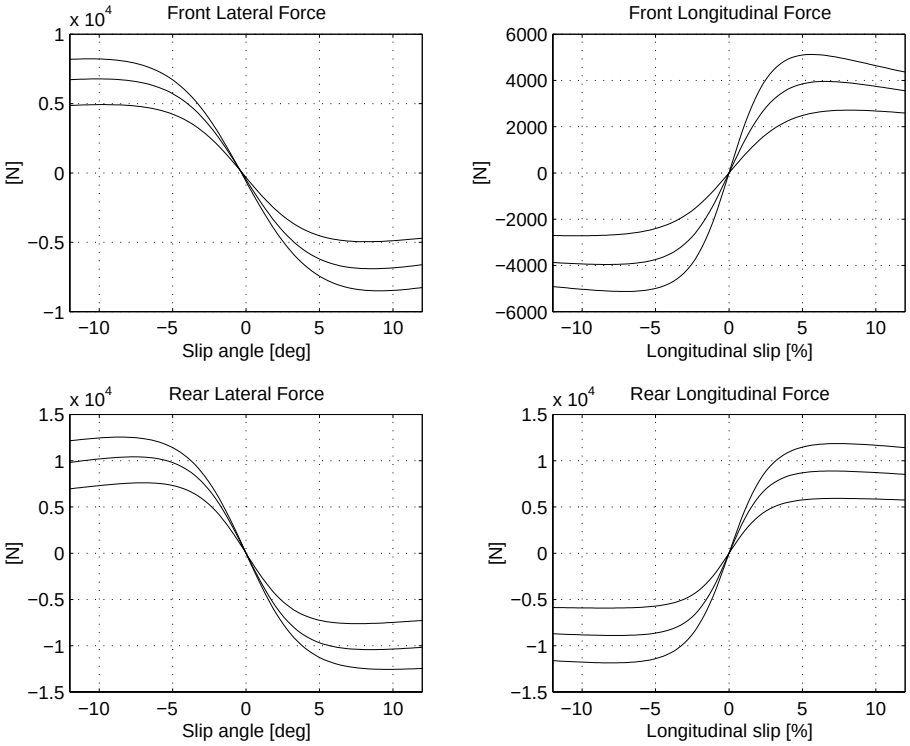

Fig. 3. Tyre force characteristics; front tyre vertical loads equal to 2, 3 and 4 kN; rear tyre vertical loads equal to 3, 4.5 and 6 kN

3.6. Vehicle model and driver model implementation

The mathematical model of a vehicle is usually described by a set of first order differential equations representing the rate of change of the system state variables **x** with respect to the time:

$$\dot{\mathbf{x}} = \mathbf{a}(\mathbf{x}, \mathbf{u}, t) \tag{5}$$

Here, **u** is the vector of the vehicle lateral and longitudinal control variables. Having specified the intended sequence of vehicle manoeuvres as a function of the path distance co-ordinate *s*, it is necessary to formulate the equations in (5) in such a way that they represent the rate of change of the states with respect to an increment of travelled distance *ds* along the ideal path. Hence, equation (5) may be modified as follows:

$$\frac{d\mathbf{x}}{ds} = S_{CF} \cdot \mathbf{a}(\mathbf{x}, \mathbf{u}, t) = \bar{\mathbf{a}}(\mathbf{x}(s), \mathbf{u}(s), s) \tag{5b}$$

where S_{CF}, whose expression is derived in Appendix 2, represents the scaling factor relating the incremental quantities *dt* and *ds*:

$$S_{CF} = \frac{dt}{ds} \tag{6}$$

The driver model uses a sub-set $\bar{\mathbf{x}}$ of the system states in order to evaluate the vehicle controls **u**. The variables required are: longitudinal and lateral position of the vehicle centre of gravity x_v and y_v, the vehicle yaw angle ψ_v and the vehicle longitudinal velocity V_{vx}:

$$\bar{\mathbf{x}} = \begin{bmatrix} x_v & y_v & \psi_v & V_{vx} \end{bmatrix}$$

Hence, the path following problem may finally be stated as follows:

$$\begin{cases} \dfrac{d\mathbf{x}}{ds} = \bar{\mathbf{a}}(\mathbf{x}(s), \mathbf{u}(s), s) \\ \mathbf{u}(s) = \mathbf{f}(\bar{\mathbf{x}}(s), s) \end{cases} \tag{7}$$

4. STEER CONTROL THROUGH PATH PREVIEW

4.1. Linear control scheme

Figure 4 shows the scheme of the multiple preview point steer angle controller. At a generic position *s* along the trajectory the driver monitors the path ahead by projecting an optical lever *L* forward, up to a distance which is chosen by the analyst to represent the extent of the preview available, giving a preview time T_P, hence making this distance a function of the vehicle velocity:

$$L = V_{vx} \cdot T_p$$

A set of n points l_1, l_2, ..., l_n is then fixed on the optical lever, the first point coinciding with the vehicle centre of gravity whose co-ordinates are $x_v(s)$ and $y_v(s)$. The vehicle attitude angle $\psi_v(s)$ determines the orientation of the optical lever and allows the calculation of the positions of the other *n-1* points. Let us next define the vector $\mathbf{\Delta_L}$ which specifies the relative distances of the points on the optical lever from the origin $x_v(s)$ and $y_v(s)$. Its i^{th} component reads:

$$\Delta_{Li} = \frac{\overline{l_i l_1}}{L} \qquad i = 1 \div n \tag{9}$$

The vector of preview distances $\mathbf{s_P}$ may then be evaluated as follows:

$$\mathbf{s_P} = L \cdot \mathbf{\Delta_L} \tag{10}$$

and, finally, the co-ordinates of the points l_1, l_2, ..., l_n read:

$$\begin{cases} \mathbf{x_L} = x_v(s) + \mathbf{s_P} \cdot \cos\left(\psi_v(s)\right) \\ \mathbf{y_L} = y_v(s) + \mathbf{s_P} \cdot \sin\left(\psi_v(s)\right) \end{cases} \tag{11}$$

From each of these points, the lateral off-set from the optical lever to the corresponding point r_1, r_2, ..., r_n on the ideal path is measured and used as input to the steer angle controller. The strategy to identify the reference points on the path ahead is chosen in order to simplify the calculations as follows: the distance of the generic point r_i measured along the ideal path from the point r_1 is taken equal to the distance between the corresponding point l_i and l_1 measured on the optical lever. Hence, the vector of preview distances $\mathbf{s_P}$ is added to the current path co-ordinate s to obtain the positions of the r_1, r_2, ..., r_n points along the path:

$$\mathbf{s_R} = s + \mathbf{s_P} \tag{12}$$

Then, the co-ordinates of these points in the axis reference system are evaluated using the matrix of path data $\mathbf{T_{RJ}}$, defined in Section 2.2, as a one dimensional look-up table with the vector $\mathbf{s_R}$ as entry value:

$$\begin{cases} \mathbf{x_R} = \text{lin\_interp}\left(\mathbf{T_{RJ}}(:,1), \mathbf{T_{RJ}}(:,4), \mathbf{s_R}\right) \\ \mathbf{y_R} = \text{lin\_interp}\left(\mathbf{T_{RJ}}(:,1), \mathbf{T_{RJ}}(:,5), \mathbf{s_R}\right) \end{cases} \tag{13}$$

Here (:,*n*) means the n^{th} column of the matrix. By following this scheme the $r_1 \div r_n$ points will not lie exactly on the direction perpendicular to the optical lever through the $l_1 \div l_n$ points and the error will be dependent on the complexity of the trajectory geometry. However, this does not seem to have any significant influence on the robustness of the driver model and this simplified approach is computationally advantageous. Having identified the set of co-ordinates ($\mathbf{x_L}$, $\mathbf{y_L}$) and ($\mathbf{x_R}$, $\mathbf{y_R}$) in the reference axis system fixed in space, the lateral off-sets e_1, e_2, ..., e_n in Figure 4 are evaluated by referring the position of each of the r_i points to a local axis system whose origin is set on the corresponding l_i points and the x local axis is oriented as the optical lever:

$$e_i = \left(y_{Ri} - y_{Li}\right)\cos\left(\psi_v\right) - \left(x_{Ri} - x_{Li}\right)\sin\left(\psi_v\right) \qquad i = 1 \div n \tag{14}$$

Of these *n* control inputs, $e_2 \div e_n$ are preview path information, whereas e_1 represents the vehicle lateral off-set from the current intended position on the path and is the first of the two state feedback inputs used by the driver model. The other state feedback signal is taken as the difference between the vehicle attitude angle and the tangent angle of the intended path at the current position *s*, which is identified by means of linear interpolation as above:

$$\begin{aligned} \psi_t &= \text{lin\_interp}\left(\mathbf{T_{RJ}}(:,1), \mathbf{T_{RJ}}(:,3), s\right) \\ e_\psi &= \psi_t - \psi_v \end{aligned} \tag{15}$$

Finally, introducing the set of control gains K_1, K_2, ..., K_n and K_ψ, the steer angle is evaluated as a linear combination of the control inputs:

$$\delta = K_\psi \cdot e_\psi + K_1 \cdot e_1 + \sum_{i=2}^{n} K_i \cdot e_i \tag{17}$$

4.2. Control law gains in relation to the system dynamics

In our approach to driver modelling there is no attempt to mimic human driver behaviour. Rather, the aim of our mathematical model is that of applying a control action based on the system dynamics in order to achieve the path following task. For this task, we refer to the theory of linear optimal control, as stated in the introduction. Such theory, when applied to vehicle suspension [11], showed that such a control scheme involves diminishing returns for extended preview and the gain sequence mirrors the system dynamics, i.e. the system is operated preferentially in its eigen-modes. Although we can not apply the same formal approach to determine the gain sequence because the vehicle model is non-linear, the theory suggests that the refer-

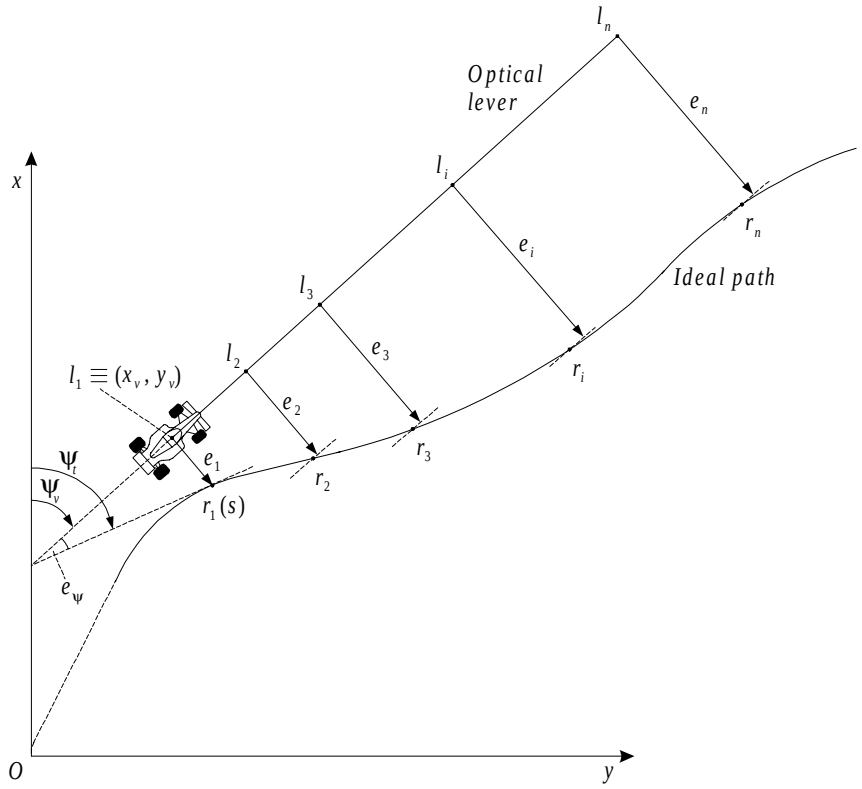

Fig. 4. Driver model scheme

ence scheme for the driver model preview gain sequence has to be exponentially convergent to zero towards distant preview samples. The vehicle on a high grip surface (e.g., race car on dry tarmac) will be a highly damped system.

The state feedback control gains proved to be very important in increasing the system stability. Especially the vehicle attitude error feedback control improved the performance of the driver model for vehicles made artificially unstable by strong oversteer. However, the contribution of the attitude error gain tends to reduce the steer angle when cornering normally, because of the natural attitude of the car in generating slip angles at the rear wheels. Hence, the vehicle runs slightly off the ideal path so that the contribution of the lateral off-set feedback control cancels out the negative contribution of the attitude error control. The two gains associated with state feedback inputs have been identified by fine tuning rather than by any formal approach, until a satisfactory performance in terms of vehicle control at limit

conditions and small path tracking error was obtained. Some guidance for the proper setting of the driver model parameters will be given at the end.

As may be seen in equations (9) and (10), the position of the preview points on the optical lever has been left as another set of parameters to choose. Although it may seem to be natural to evenly space these points along the optical lever, a different scheme might be used in view of the concept of diminishing returns, by gathering the preview points towards the vehicle centre of gravity. At this stage, such a strategy has not played a significant role, but to further refine the driver model, the distribution of the preview points along the optical lever may be varied in order to enhance computational efficiency.

4.3. Non-linear control scheme with saturation functions

The linear control law of equation (17) would correspond with linear tyre forces, but when a vehicle is operated on the limit of its performance envelope, the tyre forces saturate and any increase of the control action will be ineffective. For example, if the vehicle model were asked to follow an impossible path so that its trajectory were to depart from that path significantly, the control inputs would grow a great deal and equation (17) would return unreasonable values for the steer angle, causing the tyre forces to fall far beyond saturation. The best strategy in such conditions would be to limit the steer angle in order to keep the tyre as closely as possible to saturation, therefore maximising the control forces, until the vehicle would eventually return to the original path. In order to deal with such cases, the driver model structure is extended by including saturation functions as depicted in Figure 5. This structure is designed to handle different limit behaviour of the vehicle.

When an understeer vehicle reaches its lateral limit, its front tyres saturate first and it tends to run on a trajectory wider than the ideal path. In this situation the vehicle attitude error gives a much smaller contribution to the generation of the steer angle compared to the other preview and state feedback lateral off-set inputs. Therefore a saturation function is placed to limit the value of the sum of the contributions of all the lateral preview and state feedback off-sets. This prevents the front tyres from working too far beyond saturation, hence maximising the lateral control force to enhance the capability of the driver model to return to the original intended path. Conversely, when the rear tyres of a vehicle reach saturation first, e.g., because of its oversteer nature, or while cornering under driving or braking, the attitude error control gives the most significant contribution. In this condition the steer input required may be much larger than in the previous case of the understeer vehicle. However, to prevent the front wheels from steering beyond the physical limit of a real car, an overall saturation function is applied to the output of the driver model.

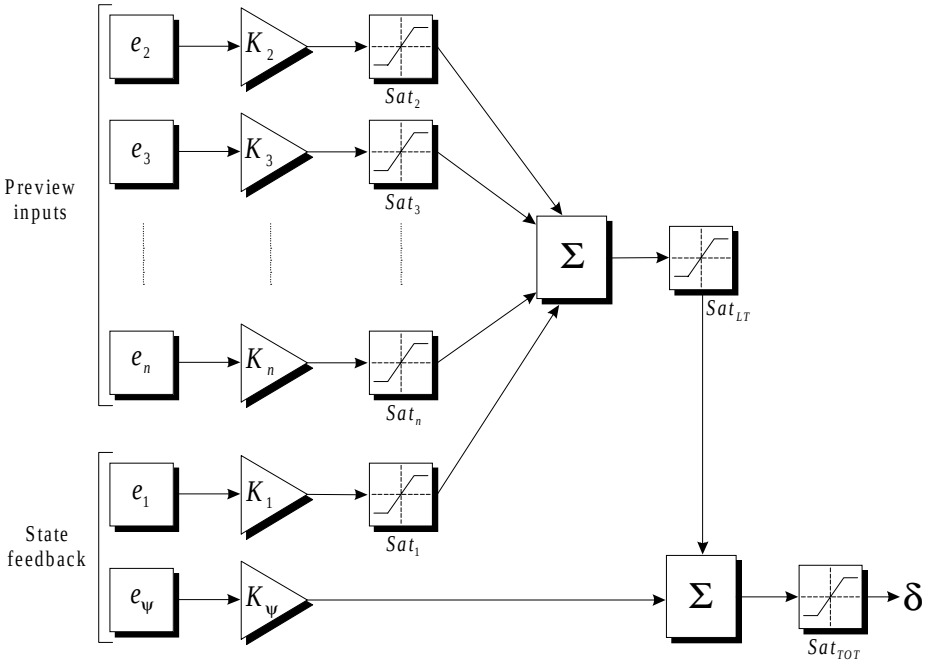

Fig. 5. Steer angle control scheme with saturation functions

If the vehicle slides temporarily away from the intended line, e.g., because of understeer, when trying to regain the original course its trajectory may cross the ideal path with a high angle of incidence. In this condition the simple linear structure of equation (17) plus the global saturation functions would return a steep shift of the steer angle from the maximum to the minimum value and vice versa, hence inducing some oscillations before the vehicle may recover the original course on the ideal path. To further improve the driver model response in such extreme manoeuvres, the contribution to the steer angle generation from each of the preview and lateral state feedback inputs is limited by applying individual saturation functions. This scheme has a more progressive action in such extreme conditions and improves the capability of the driver model to deal with limit manoeuvres. The final scheme of the multiple preview points steer angle control of Figure 5 includes n+2 more parameters, the individual saturation levels Sat_i and the global ones Sat_{LT} and Sat_{TOT}, whose values will be discussed at the end.

5. SPEED CONTROL SCHEME

5.1. Vehicle longitudinal inverse dynamics

Among the possible schemes for the vehicle longitudinal control described in section 2.1, the one adopted here consists in specifying a variable longitudinal velocity along the ideal path, and determining the vehicle longitudinal thrust by solving a simple one dimensional inverse dynamics problem. Let us consider the vehicle travelling with a velocity $V_{vx}(s)$ at a generic position s along the ideal path. From the current position the driver model reads the target velocity from the ideal velocity profile at a short distance ahead, $V_t(s+\Delta s)$. The constant acceleration which would be required to reach the target velocity may now be evaluated:

$$a(s) = \frac{\left[V_t(s+\Delta s) - V_{vx}(s)\right]}{\Delta s} \cdot \frac{1}{S_{CF}} \tag{18}$$

Here the scaling factor S_{CF} is required to obtain the time derivative of the velocity. The longitudinal force F that is required to maintain the ideal forward motion may now be evaluated as follows:

$$F(s) = M \cdot a(s) + J_f \cdot \frac{a(s)}{R_f^2} + \left(J_r + J_m \cdot G_r^2\right) \cdot \frac{a(s)}{R_r^2} + \frac{1}{2}\rho \cdot S \cdot C_x \cdot V_{vx}^2(s) \tag{19}$$

Here, the first term is the inertia due to the mass of the vehicle, the second term is the inertia of the front axle rotating masses, the third term is the inertia of the rear axle rotating masses plus the inertia due to the engine, which depends on the gear ratio G_r, and the last term is the aerodynamic drag. Other smaller effects like the drag induced by the steering wheels in cornering may be neglected with little loss in accuracy, since the speed control scheme works as a simple feedback control and is therefore self correcting.

Finally, the torque applied to the front and rear axles may be evaluated according to the vehicle model configuration. When F is positive (driving), all the torque is applied to the rear axle:

$$T_r = F \cdot R_r; \qquad T_f = 0 \tag{20}$$

When F is negative (braking), the contribution of the engine negative output torque at closed throttle is taken into account, since it has a significant influence on the braking balance. The gear ratio G_r, which is selected upon the vehicle forward velocity, allows the evaluation of the engine rotational velocity and then the engine braking torque E_{brk} is evaluated from the experimentally determined engine map. If

the negative forward force is less than the engine braking effect, braking torque is only applied to the rear axle:

$$T_r = F \cdot R_r; \qquad T_f = 0 \qquad if \quad |F| \le \left| \frac{E_{brk} \cdot G_r}{R_r} \right| \tag{21}$$

Otherwise, the residual negative force F_{res}, the amount by which the total exceeds the engine braking effect, is applied through the vehicle brakes. The constant parameters B_f and B_r determine the fixed ratio of the braking torque applied to the front and rear axles. Equations (23) allow the evaluation of the control torques to be applied to the vehicle axles, taking into account different front and rear wheel radii.

$$F_{res} = F - \frac{E_{brk} \cdot G_r}{R_r} \tag{22}$$

$$T_f = F_{res} \cdot \frac{R_f \cdot R_r \cdot B_f}{R_r \cdot B_f + R_f \cdot B_r}; \qquad T_r = E_{brk} \cdot G_r + F_{res} \cdot \frac{R_f \cdot R_r \cdot B_r}{R_r \cdot B_f + R_f \cdot B_r} \tag{23}$$

5.2. Infeasible manoeuvres: exception handling

Although the driver model has proved to be capable of controlling the vehicle in many extreme conditions, as we show in the next section, decoupling the vehicle longitudinal control from the lateral control implies the possibility of infeasible manoeuvres. Exceptional conditions may occur when the ideal velocity profile is impossible, in view of tyre force saturation. When the path following task is compromised, it is convenient to have a method to detect such a condition and to stop the simulation, returning the results which allow one to understand what has happened. In order to do this, the value of the scaling factor S_{CF} is monitored during the simulation. When the vehicle follows closely the ideal path, the value of the scaling factor is almost equal to the inverse of the velocity:

$$S_{CF} = \frac{dt}{ds} \cong \frac{1}{V_{vx}} \tag{24}$$

But if the vehicle drifts away from the ideal path or tends to spin off, equation (24) does not hold any longer. In the limit case that the vehicle trajectory becomes perpendicular to the ideal path, the increment of travelled distance *ds* along the latter would be zero for any variation of the vehicle states, the scaling factor would become infinite and the equations of motion of the vehicle singular. If, instead, the vehicle

trajectory lies inside the ideal path through a corner, the opposite situation may occur, with the scaling factor being smaller than the value predicted by equation (24).

Exception handling is realised by allowing a certain range of variation of the scaling factor as a measure of good path following. When the scaling factor exceeds the set limits the simulation is stopped and the results returned up to the final vehicle position, in order to detect what caused the driver model to fail. A proper range of variation of the scaling factor has been found to be approximately 50 % of the inverse of the vehicle velocity.

6. PATH FOLLOWING TRIALS

In this section various path following tasks of increasing difficulty are set in order to prove the effectiveness of our driver model. The vehicle parameters and the tyre model are referred to those of a Formula One single-seater race car according to the 1997 technical specifications.

6.1. Moderate 'g' manoeuvres: double lane change

An ideal path representing a double lane change manoeuvre has been generated by defining a curvature function varying between 0 and 0.04, corresponding to a minimum cornering radius of 25 meters, Figure 6. The intended vehicle longitudinal velocity has been set equal to a constant value of 18 meters per second. This implies a lateral acceleration at the apex of the turn of about 1.3 g, which is not very demanding for a Formula One car. The first graph of Figure 6 shows the vehicle trajectory superimposed on the ideal path. The two lines are actually indistinguishable and only the second graph reveals a maximum path tracking error of 0.04 m.

The vehicle model completes the manoeuvre maintaining the ideal velocity as the second plot in Figure 7 shows. Only when the vehicle is cornering is there a small error due to the fact that the speed control scheme does not account for the drag induced by the steering of the road wheels. Finally, Figure 8 shows that the level of tyre lateral saturation (see Appendix 1) does not exceed 52 %.

6.2. High 'g' manoeuvres: Lap simulation

A set of data including vehicle velocity, lateral acceleration and steer angle round a lap at Suzuka circuit was available from the 1997 Japanese Grand Prix. Using the method outlined in section 2.2, the racing line of the real car has been reconstructed. Then, the driver model has been asked to follow this path at racing speed. Figure 9, together with the first plot of Figure 10, shows the excellent path tracking capability of the driver model, with a maximum vehicle lateral off-set of the order of 0.2 m. Figure 11 shows the good agreement between the steer angle measured on board the

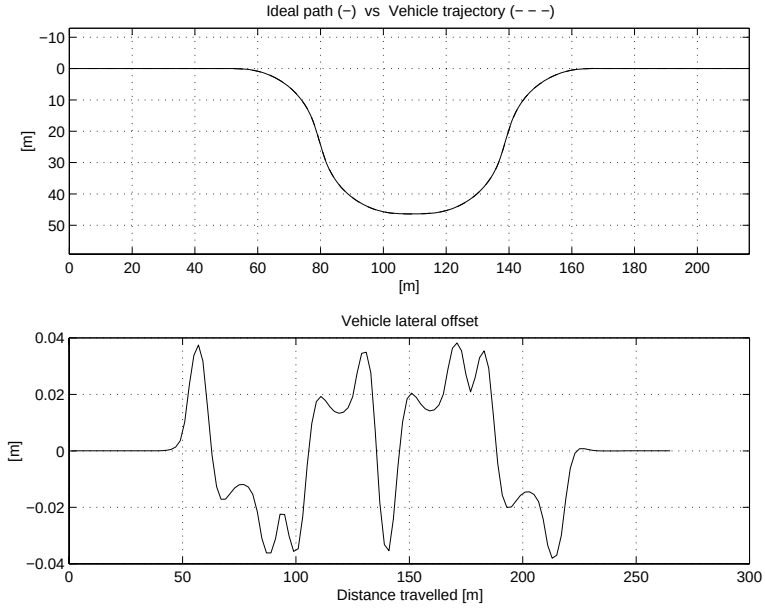

Fig. 6. Double lane change manoeuvre path tracking result

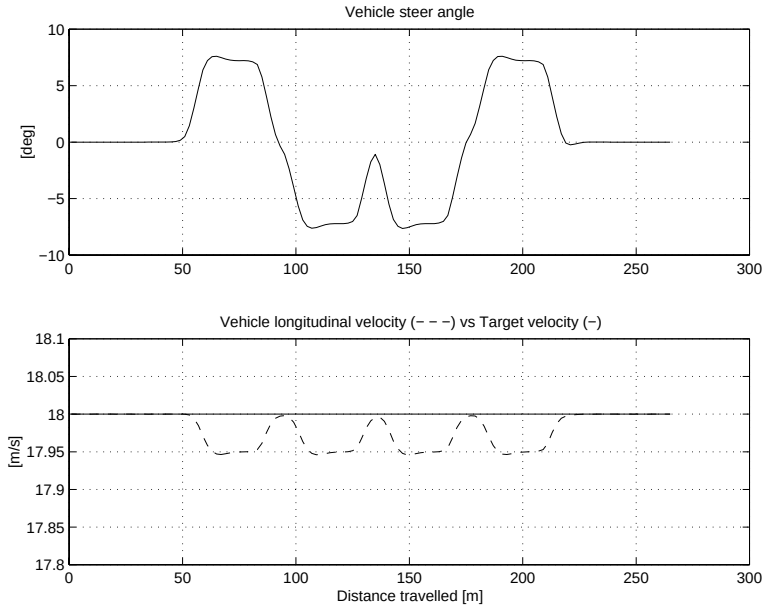

Fig. 7. Steer angle control and vehicle longitudinal velocity control

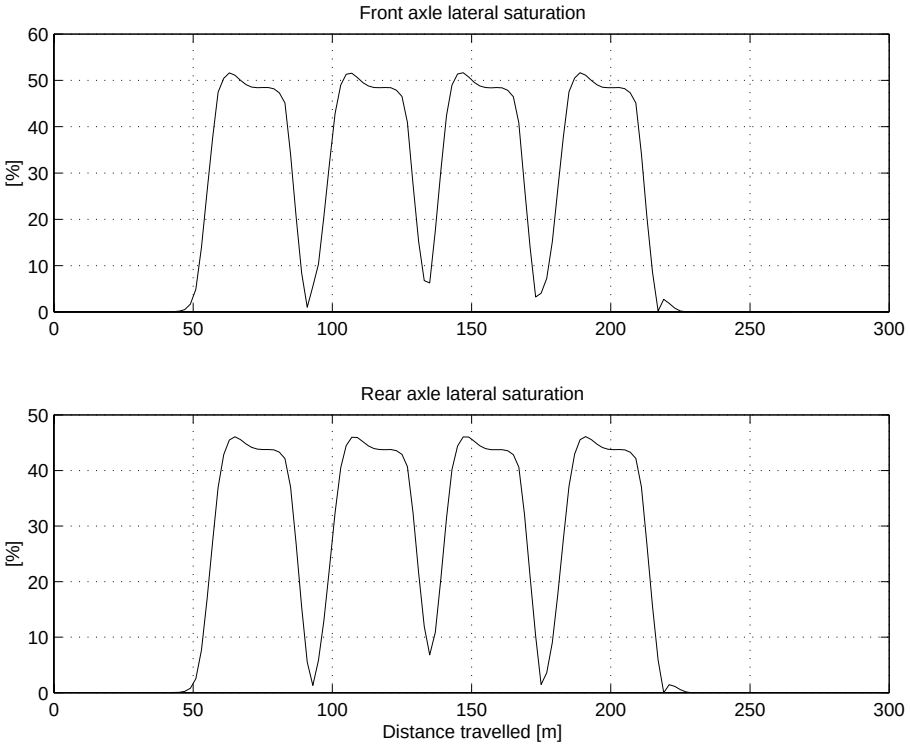

Fig. 8. Tyre lateral saturation levels

car and the steer angle returned by the driver model. The target velocity is matched very well throughout the whole lap, as the second plot of Figure 10 shows, although the use of real data, which may still include some noise even after filtering, causes the control torque to be rather noisy as well, as may be seen in Figure 12. Finally, Figures 13 and 14 represent the tyre saturation levels (see Appendix 1) in both longitudinal and lateral directions, which come very close to 100 %, indicating that the vehicle model is mostly working deep into the non-linear region of its tyres.

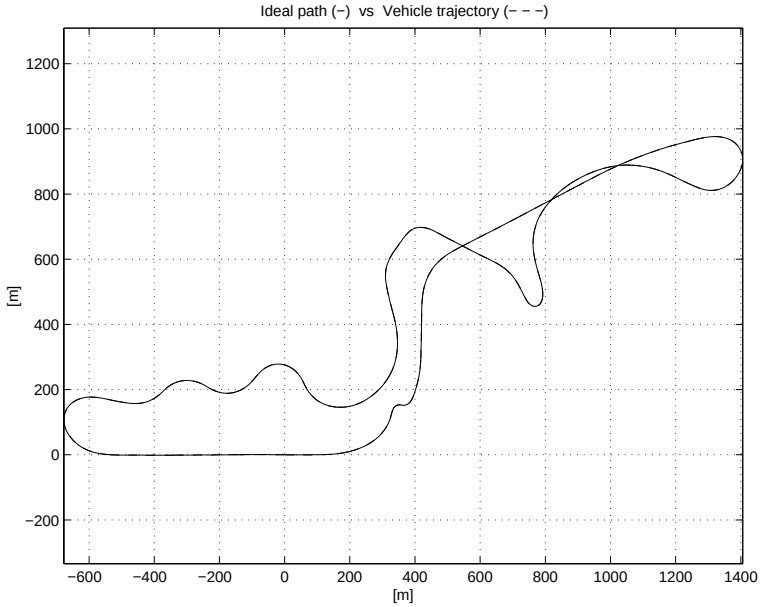

Fig. 9. Racing line path following task results

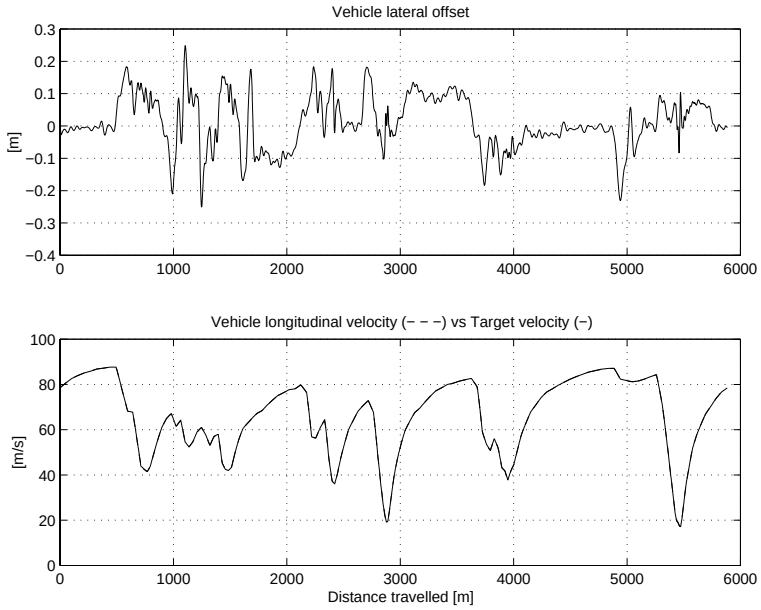

Fig. 10. Path tracking error and vehicle longitudinal velocity

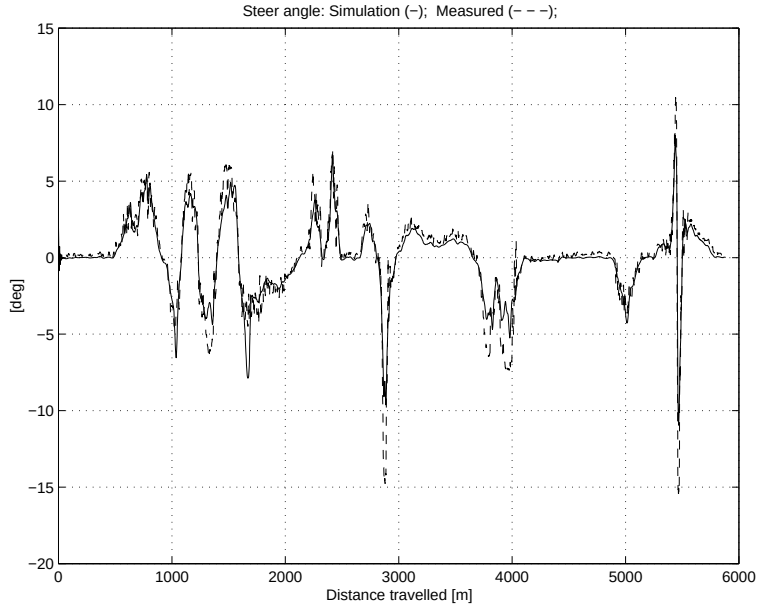

Fig. 11. Vehicle steer angle control

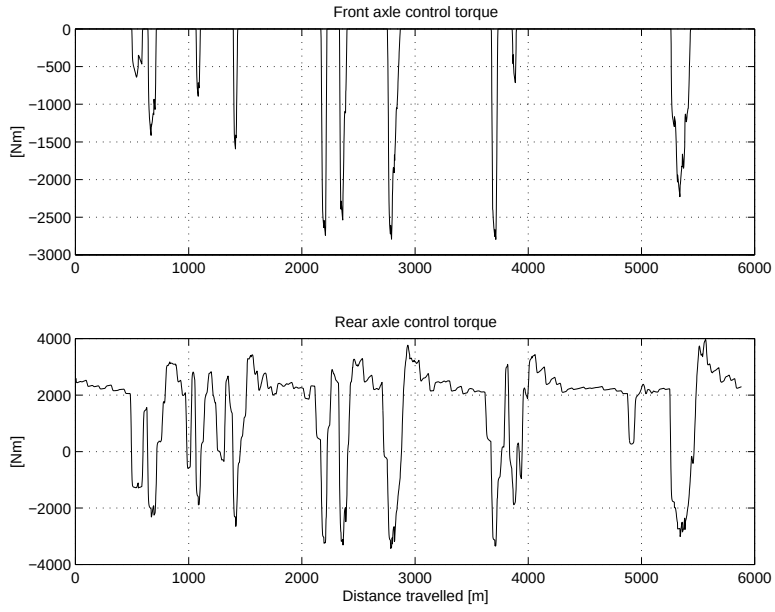

Fig. 12. Driving and braking control torques

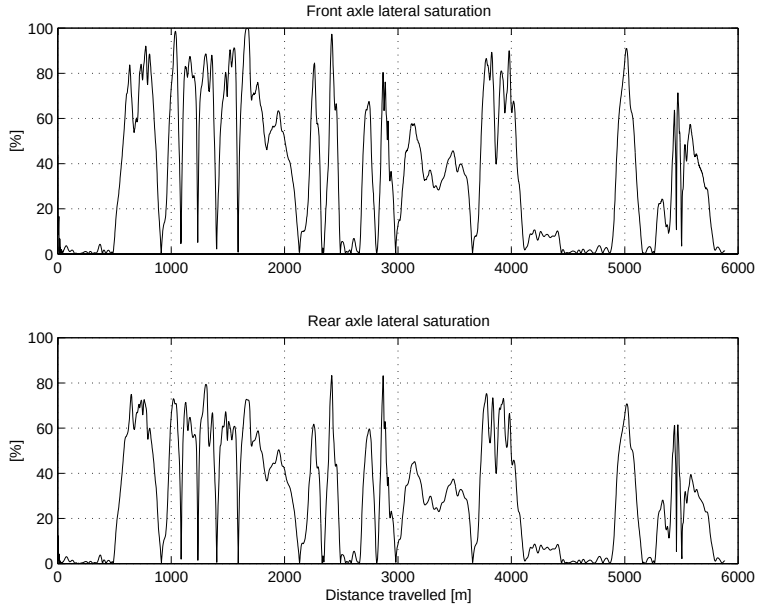

Fig. 13. Tyre lateral saturation levels

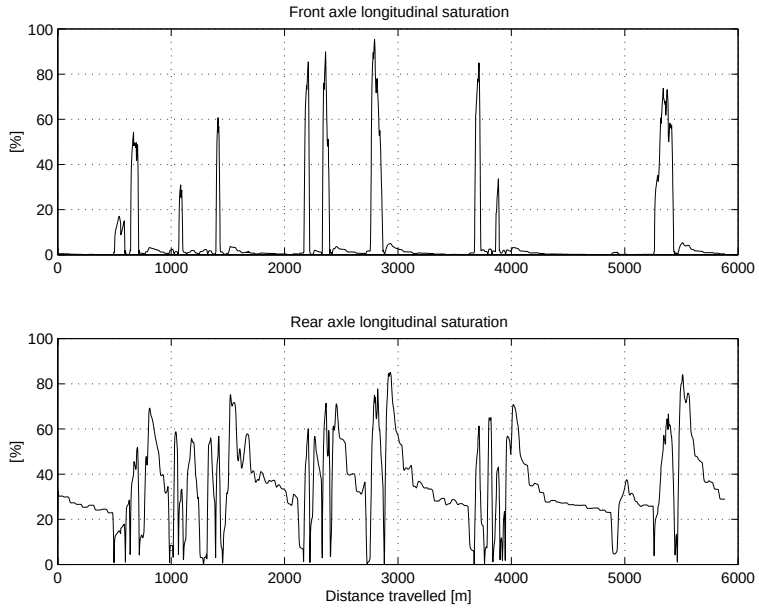

Fig. 14. Tyre longitudinal saturation levels

6.3. Limit manoeuvres: understeer and oversteer vehicles

In order to show the robustness of the driver model in extreme conditions, the vehicle model parameters have been altered in order to change its limit behaviour. The vehicle parameters which influence the load distribution among the tyres, e.g., roll stiffness distribution and aerodynamic downforce distribution between the front and rear axles, have been changed in order to make the vehicle very unbalanced, firstly towards understeer behaviour, then towards oversteer behaviour. Figures 15, 16 and 17 refer to the understeer vehicle. The trajectory is the initial section of the same racing line around the Suzuka circuit used in the previous example. The results show that on two occasions the vehicle leaves the ideal path and drifts towards the right hand side with a significant path tracking error. However, in both cases, even after large excursions from the intended trajectory, the driver model is capable of regaining the original course without any oscillation. In this condition the saturation functions play a significant role by preventing the steer angle from exceeding a reasonable range. This prevents the front tyres from working too far beyond lateral saturation, hence maximising the capability of the vehicle lateral control. Figure 17 shows that the front tyre lateral force saturates, while the rear tyres are only working at 60 % of their capability. Figures 18, 19 and 20 refer to the oversteer vehicle. Path tracking is not a problem in this case, as the vehicle trajectory is almost indistinguishable from the ideal path. The second graph in Figure 19 shows the side-slipping attitude of the vehicle throughout the whole section, with the rear tyres of the vehicle working with a larger slip angle than the front tyres. Figure 20 shows also that in this case the rear tyres are working on their friction limit, while the front tyres are only using up to 70 % of their capability. The steer angle results show that the oversteering vehicle requires far less steer angle input to complete the manoeuvre than the actual car, as is expected, and also that the driver has to apply opposite steer angle in order to control the vehicle.

6.4 .General rules for setting the driver model parameters

The setting up of the driver model parameters involves two phases. Firstly, a set of initial values for the gains is derived by proceeding as follows. Several open-loop simulations are done by setting constant values of the steer, throttle and brake controls each time. Then, using the values of the vehicle state variables, the optical lever is projected from several fixed positions on the simulated trajectories in order to read what would be the input to the controller. In order to do this, the initial structure of the driver steering control must be defined in terms of preview time, the number of preview points and their positions along the optical lever. For the current implementation the preview time has been set equal to one second and 8 points have been placed on the optical lever, including the one which accounts for the state feedback

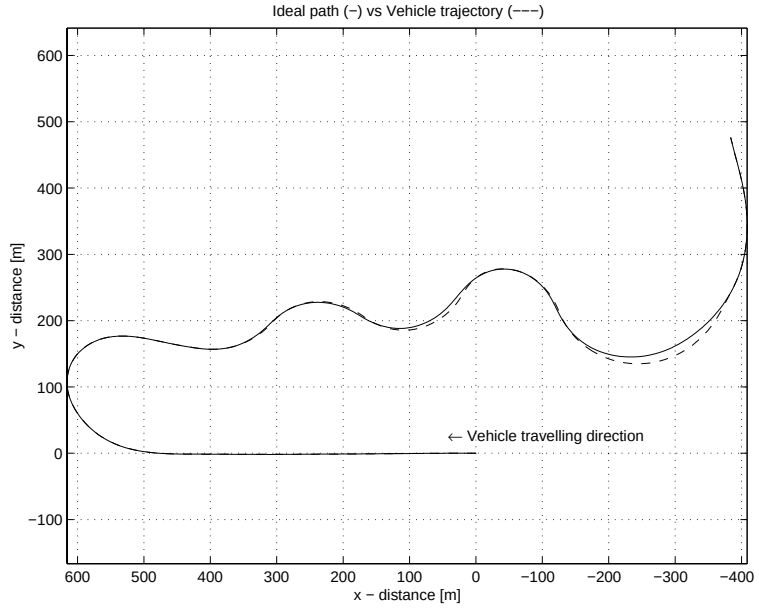

Fig. 15. Path tracking results from understeer vehicle

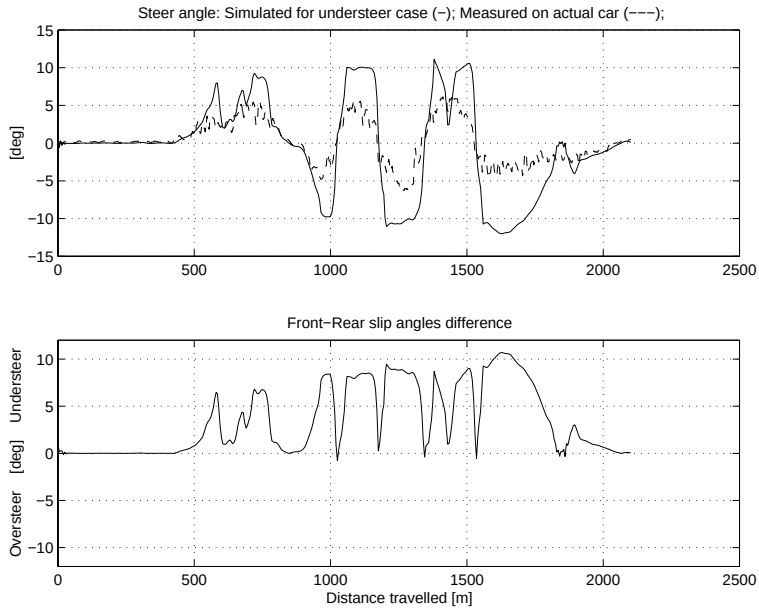

Fig. 16. Vehicle steer angle control and vehicle attitude, understeer vehicle

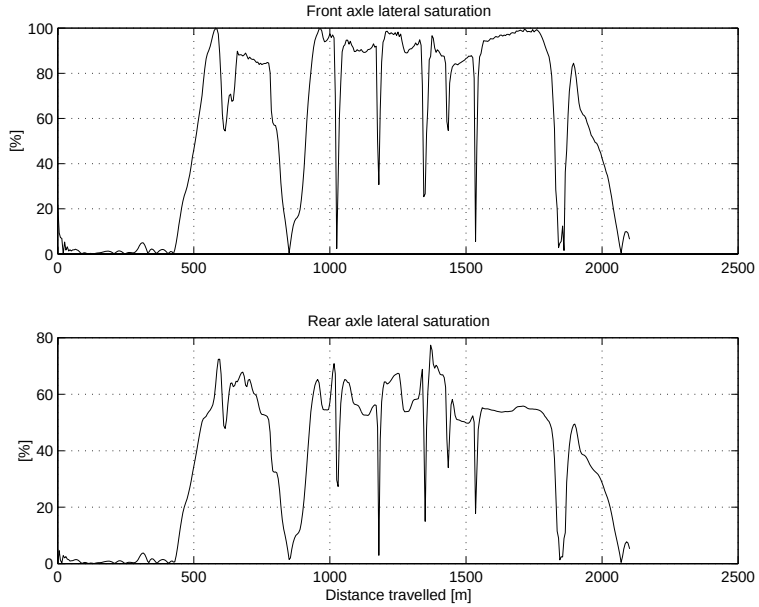

Fig. 17. Tyre lateral saturation levels for understeer vehicle

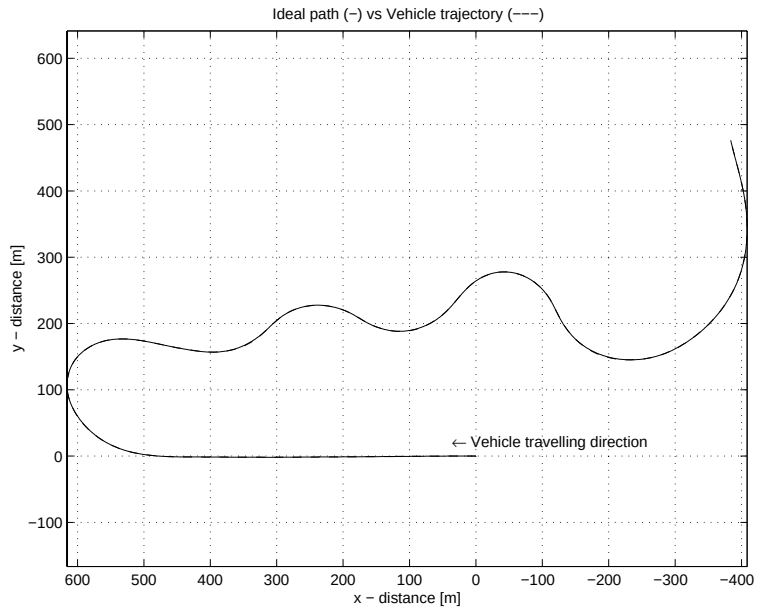

Fig. 18. Path tracking results from oversteer vehicle

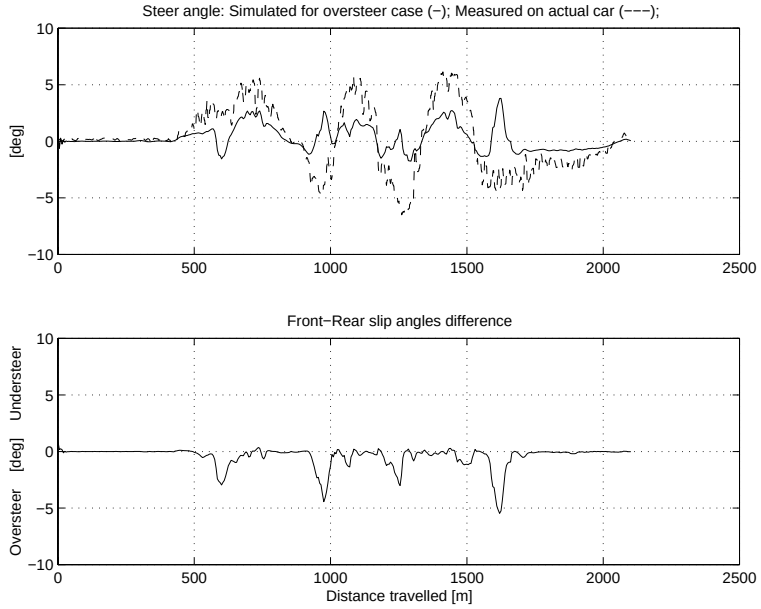

Fig. 19. Vehicle steer angle control and vehicle attitude, oversteer vehicle

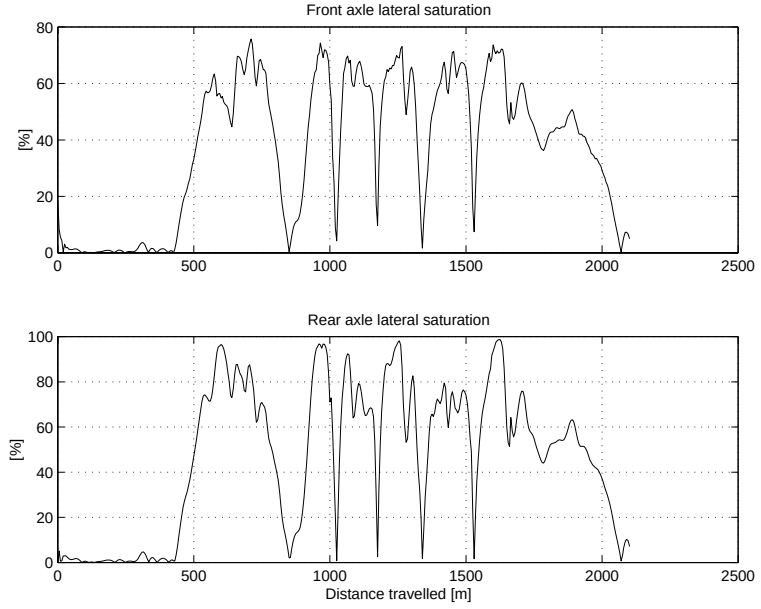

Fig. 20. Tyre lateral saturation levels for oversteer vehicle

lateral off-set. Furthermore, the first four preview points have been gathered towards the origin of the optical lever, although it is not clear at the moment whether this scheme is really advantageous, as explained in Section 4.2. Once the controller inputs corresponding to a certain steer angle are known, the gains to generate such value for the steer angle may be estimated on the basis of the exponential diminishing returns scheme. For example, the contribution of the first preview input (e_2 in Fig. 4) may be set equal to the 30 % of the total steer angle, that of the second preview point equal to the 15 %, then 10 %, 5 % end so on. Less information may be given about the initial setting of the state feedback gains. A good estimate to begin with is to set them equal to the numerical value of the first preview gain.

The second phase consists in tuning the set of parameters of the driver model in order to minimise the path tracking error and to improve the vehicle control in limit manoeuvres. Increasing the attitude error gain usually improves the control of unstable vehicles. As a consequence, this may result in a larger path tracking error since the contribution of the attitude error control tends to reduce the steer angle when the vehicle is cornering normally as was explained in Section 4.2. The state feedback lateral off-set control gain may be used to compensate this effect. The setting of the saturation levels may be done at this stage, since their influence is relevant only in extreme conditions. The total saturation is usually set equal to the maximum steer angle achievable by the real car in order to prevent the driver model from returning absurd values. The saturation function which is applied to the sum of the contributions of all the preview and state feedback lateral off-sets is more relevant when controlling understeer vehicles, as shown in Section 6.3. In such conditions the steer angle should be limited to a value which sets the front tyres working at a slip angle which is as close as possible to that at maximum lateral saturation, in order to maximise the control force. However, the proper value varies depending on the kinematic conditions, tyre vertical loads, etc., hence the choice will be made in order to compromise the driver response in several different manoeuvres. Finally, the individual saturation levels have the function of smoothing the action of the driver model when trying to regain the ideal path after large excursions from the intended line like that shown in Figure 15. As a general rule it may be indicated that the contribution from each of the lateral off-set controls should not be greater than the 10 ÷ 20 % of the maximum steer angle allowed. Table 1 reports all the values of the parameters of the driver model currently implemented. It has been found necessary to change these values infrequently.

7. CONCLUSIONS AND FURTHER RESEARCH

A new structure for a steering controller for a road vehicle has been devised. The controller takes in sample values of preview path errors, lateral position error and attitude error and converts the observations into a steering wheel angle control. The structure is based in optimal linear discrete time preview control theory but it has

Table 1. Driver model parameters.

Lateral off-set control parameters			
Index	Relative Position	Gain [deg/m]	Saturation level [deg]
i	Δ_{Li}	K_i	Sat_i
1	0	10	±1
2	0.1	10	±2
3	0.2	6	±2
4	0.3	2	±2
5	0.4	0.8	±2
6	0.6	0.16	±1
7	0.8	0.04	±1
8	1	0.01	±1
Attitude error control gain, $K\psi$			30 [deg/rad]
Total lateral off-set control saturation level, Sat_{LT}			±10 [deg]
Global saturation level, Sat_{TOT}			±16 [deg]

been developed to deal with non-linear vehicle operation arising from the inevitable tyre force saturation in vigorous manoeuvring. Steering controller gain and saturation parameters have been chosen by heuristic methods and some procedures by which this can be done effectively have been established. Important features of the model are that it uses both feedback and preview control and that it uses multi-point preview.By association of the steering controller with moderate manoeuvring and race car level operations of varied nature, the accuracy of the steering controller and its robustness (without parameter changes) to changes in vehicle or task have been demonstrated.

In the linkage of the steering controller to a vehicle dynamics simulation model, the transformation of the problem from time domain to distance domain is seen as important. The transformation method used is in advance of previous work and it has contributed usefully to the outcome. It has also allowed a convenient check on the health of a simulation run to be incorporated into the calculations, mitigating against wasted runs.

Although based in linear discrete-time optimal control theory, the steering control structure is similar to that of a neural network, so it seems likely that the parameter tuning process will be achievable in future by standard neural network learning procedures [12]. In such a form, the steering controller appears to have close parallels with human drivers and it appears possible that the learning process itself will be interesting. It may even transpire that the control qualities of a vehicle may be capable of assessment by observation of the ‘driver’ learning process. At the present time with real drivers, such observations are, of course, not possible. Another issue for further work is modelling the driver’s longitudinal control activity, leading to the design of a coupled longitudinal/lateral scheme.

REFERENCES

1. Allen, J. B., Computer optimisation of cornering line, Cranfield University, School of Mechanical Engineering, M.Sc. Thesis, 1997.
2. Bernard, J. and Pickelmann, M., An inverse linear model of a vehicle, Vehicle System Dynamics, 15(4): 179-186, 1986.
3. Chiesa, A., Rinonapoli, L. and Bergomi, P. I. R., A new loose inverse procedure for matching tyres and car using a mathematical model, Handling of Vehicles under Emergency Conditions, Proc. I. Mech. E., 183(3H): 49-64, 1969.
4. Dixon, J. C., Tyres, Suspension and Handling, Society of Automotive Engineers, Inc., 1996, Second edition.
5. Garrott, W. R., Wilson, D. L. and Scott, R. A., Closed loop automobile maneuvers using describing function models, SAE 820306, 1982.
6. Guo, K. and Guan, H., Modelling of driver/vehicle directional control system, Vehicle System Dynamics, 22(3-4): 141-184, 1993.
7. Katayama, T., Nishimi, T., Okayama, T. and Aoki, A., A simulation model for motorcycle rider's control behaviour, Proc. SETC '97, Society of Automotive Engineers of Japan, Inc., 373-382, 1997.
8. MacAdam, C. C., Application of an optimal preview control for simulation of closed-loop automobile driving, IEEE Transactions on Systems, Man and Cybernetics, SMC-11(6), 393-399, June 1981.
9. MacAdam, C. C. and Johnson, G. E., Application of elementary neural networks and preview sensors for representing driver steering control behaviour, Vehicle System Dynamics, 25(1): 3-30, 1996.
10. Pacejka, H. B. and Besselink, I. J. M., Magic Formula tyre model with transient properties, in Tyre Models for Vehicle Dynamics Analysis, (F. Böhm and H. – P. Willumeit eds), Suppl. Vehicle System Dynamics 27: 234-249, 1997.
11. Sharp, R. S., Preview control of active suspensions, Smart Vehicles, J. P. Pauwelussen and H. B. Pacejka eds, Swets and Zeitlinger, 166-182, 1995.
12. Tarassenko, L., A guide to neural computing applications, Arnold, London (co-published by John Wiley for the Americas), 1998.
13. Weir, D. H. and McRuer, D. T., A theory for driver steering control of motor vehicles, Highway Research Record, 247: 7-39, 1968.

APPENDIX 1. VEHICLE MODEL EQUATIONS

Referring to figs 21 and 22, the equations of motion of the vehicle model read (for the meaning of the symbols see Table 2):

$$
\begin{aligned}
\dot{x}_1 &= x_2 \\
\dot{x}_2 &= \left[\left(F_{fy}\cos(\delta) + F_{fx}\sin(\delta)\right)l_f - F_{ry}l_r\right]\frac{1}{I_z} \\
\dot{x}_3 &= \left[F_{fx}\cos(\delta) - F_{fy}\sin(\delta) + F_{rx} - F_{ax}\right]\frac{1}{M} + x_2 x_4 \\
\dot{x}_4 &= \left[F_{fy}\cos(\delta) + F_{fx}\sin(\delta) + F_{ry}\right]\frac{1}{M} - x_2 x_3 \\
\dot{x}_5 &= x_3\cos(x_1) - x_4\sin(x_1) \\
\dot{x}_6 &= x_3\sin(x_1) + x_4\cos(x_1) \\
\dot{x}_7 &= x_8 \\
\dot{x}_8 &= \left(T_r - F_{rx}R_r\right)\frac{1}{\left(J_r + J_m \cdot G_r^2\right)} \\
\dot{x}_9 &= x_{10} \\
\dot{x}_{10} &= \left(T_f - F_{fx}R_f\right)\frac{1}{J_f}
\end{aligned}
\tag{25}
$$

The aerodynamic drag and down-force in equations (25) are evaluated as follows:

$$
\begin{aligned}
F_{ax} &= \frac{1}{2}\rho\, SC_x x_3^2 \\
F_{az} &= \frac{1}{2}\rho\, SC_z x_3^2
\end{aligned}
\tag{26}
$$

The vertical load acting on each wheel is evaluated including a steady state approximation of the lateral and longitudinal load transfers. Firstly, the static distribution of the vehicle weight and the aerodynamic down-force on the front and rear axles is calculated as follows:

$$
\begin{aligned}
F_{fz\_static} &= \left(M \cdot g \cdot l_r + F_{az} \cdot d_r\right) / W_b \\
F_{rz\_static} &= \left(M \cdot g \cdot l_f + F_{az} \cdot d_f\right) / W_b
\end{aligned}
\tag{27}
$$

Then, the longitudinal load transfer, which occurs in driving or braking conditions, is evaluated by considering the equilibrium of the vehicle about its centre of gravity. Assuming the aerodynamic drag acts at the height of the CG, the expression for the longitudinal load transfer reads:

$$\Delta F_{z\_long} = \left(F_{fx} + F_{rx}\right)\frac{h_g}{W_b} \cong \left(\frac{T_f}{R_f} + \frac{T_r}{R_r}\right)\frac{h_g}{W_b} \tag{28}$$

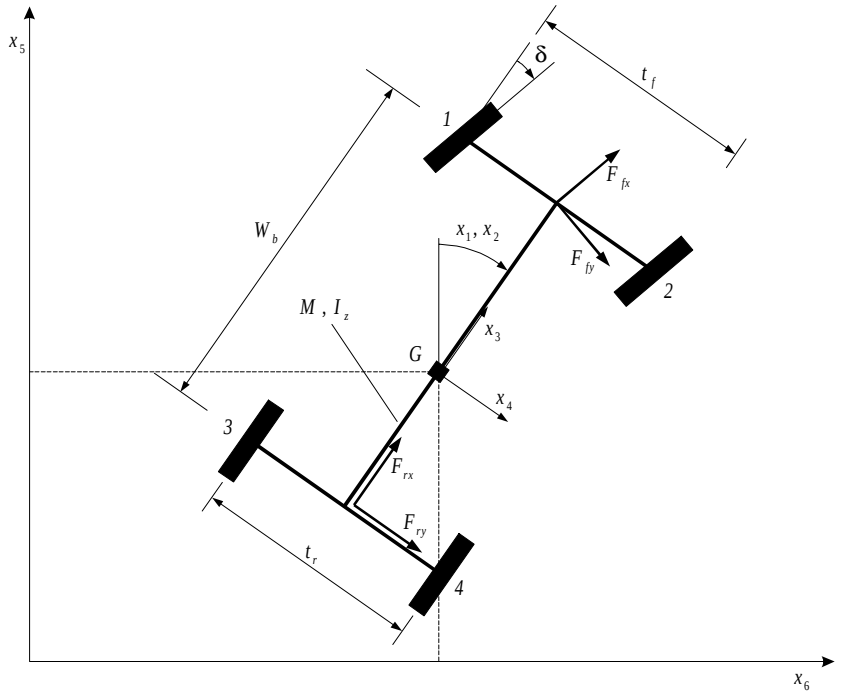

Fig. 21. Top view of the vehicle model

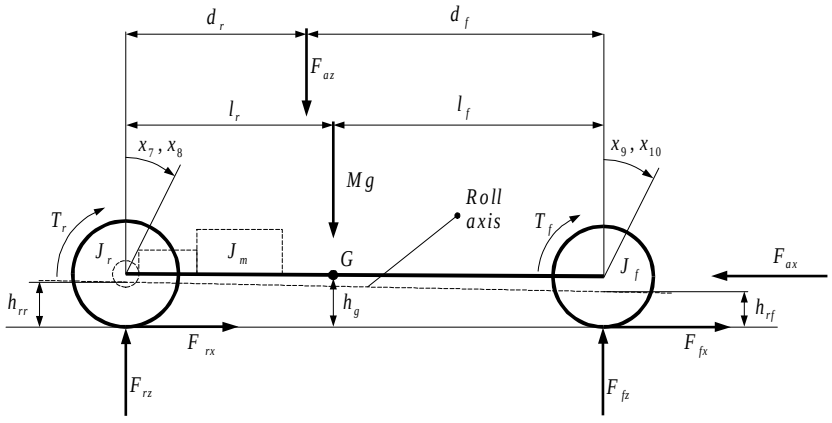

Fig. 22. Side view of the vehicle model

Table 2. Variable list.

VEHICLE MODEL STATE VARIABLES		
Yaw angle	x_1	[rad]
Yaw rate	x_2	[rad/s]
Longitudinal velocity (local reference system)	x_3	[m/s]
Lateral velocity (local reference system)	x_4	[m/s]
Longitudinal position (global reference system)	x_5	[m]
Lateral position (global reference system)	x_6	[m]
Rear wheels angular position	x_7	[rad]
Rear wheels angular velocity	x_8	[rad/s]
Front wheels angular position	x_9	[rad]
Front wheels angular velocity	x_{10}	[rad/s]
VEHICLE MODEL PARAMETERS		
Vehicle mass	M	[kg]
Vehicle yaw inertia	I_z	[kg·m^2]
Front axle polar moment of inertia	J_f	[kg·m^2]
Rear axle polar moment of inertia	J_r	[kg·m^2]
Engine moment of inertia	J_m	[kg·m^2]
Wheel base	W_b	[m]
CG height	h_g	[m]
Distances of the centre of gravity from the front and rear axles	l_f, l_r	[m]
Distances of the centre of application of the aerodynamic down-force from the front and rear axles	d_f, d_r	[m]
Front and rear roll centre heights	h_{rf}, h_{rr}	[m]
Front and rear roll stiffness proportions	R_{sf}, R_{sr}	[%]
Front and rear wheel radii	R_f, R_r	[m]
Front and rear tracks	t_f, t_r	[m]
Frontal area	S	[m^2]
Aerodynamic drag coefficient	C_x	-
Aerodynamic lift coefficient	C_z	-
Gear ratio	G_r	-
VEHICLE MODEL FORCES AND TORQUE		
Front axle lateral force	F_{fy}	[N]
Front axle longitudinal force	F_{fx}	[N]
Rear axle lateral force	F_{ry}	[N]
Rear axle longitudinal force	F_{rx}	[N]
Aerodynamic drag	F_{ax}	[N]
Aerodynamic down force	F_{az}	[N]
Vehicle weight	Mg	[N]
VEHICLE MODEL CONTROL VARIABLES		
Steer angle	δ	[deg]
Front axle torque	T_f	[Nm]
Rear axle torque	T_r	[Nm]
CONSTANTS		
Gravitational acceleration	g	[m/s^2]
Air density	ρ	[kg/m^3]

Since the longitudinal axles forces are functions of the tyre vertical loads and therefore unknown, their values are approximated by substituting the torque applied to the front and rear wheels. In doing this, the contribution of the inertia of the rotating masses is neglected and the longitudinal load transfer will be slightly overestimated. Finally, the lateral load transfer is estimated by evaluating the steady state cornering equilibrium of the vehicle, assuming a fixed roll axis position and a constant roll stiffness distribution [4]. Neglecting the contribution of the unsprung masses, the expressions of the lateral load transfer for the front and rear axles read respectively:

$$\begin{aligned}\Delta F_{fz\_lat} &= \frac{x_2 \cdot x_3 \cdot M}{t_f}\left[\left(l_r \cdot h_{rf}\right) / W_b + R_{sf}\left(h_g - h_{rc}\right)\right] \\ \Delta F_{rz\_lat} &= \frac{x_2 \cdot x_3 \cdot M}{t_r}\left[\left(l_f \cdot h_{rr}\right) / W_b + R_{sr}\left(h_g - h_{rc}\right)\right]\end{aligned} \tag{29}$$

Here, h_{rc} is the roll axis height at the position of the vehicle centre of gravity. The vertical load on each wheel may now be evaluated. According to the SAE conventions, which implies negative tyre loads, we may write:

$$\begin{aligned}F_{z1} &= -\left[\frac{1}{2}F_{fz\_static} - \frac{1}{2}\Delta F_{z\_long} + \Delta F_{fz\_lat}\right] \\ F_{z2} &= -\left[\frac{1}{2}F_{fz\_static} - \frac{1}{2}\Delta F_{z\_long} - \Delta F_{fz\_lat}\right] \\ F_{z3} &= -\left[\frac{1}{2}F_{rz\_static} + \frac{1}{2}\Delta F_{z\_long} + \Delta F_{rz\_lat}\right] \\ F_{z4} &= -\left[\frac{1}{2}F_{rz\_static} + \frac{1}{2}\Delta F_{z\_long} - \Delta F_{rz\_lat}\right]\end{aligned} \tag{30}$$

The tyre forces are evaluated by using the Magic Formula Tyre Model which features the use of weighting functions to represent the tyre behaviour at combined slip conditions [10]. We may formally write:

$$\begin{cases}F_{yi\,(combined)} = F_{yi\,(free\ rolling)}\left(\alpha_i, \gamma_i, F_{zi}\right) \cdot G_y\left(\alpha_i, k_i, \gamma_i, F_{zi}\right) \\ F_{xi\,(combined)} = F_{xi\,(pure\ slip)}\left(k_i, F_{zi}\right) \cdot G_x\left(\alpha_i, k_i\right)\end{cases} \quad i = 1,2,3,4 \tag{31}$$

A value for the static camber γ_i is assigned to each wheel. The tyre slip quantities are evaluated with the assumption of small angles and they are referred to the centre of the front and rear axles, as for a bicycle model, so that they will be the same for the

wheels sharing an axle. The expressions for the slip angles in degrees and the longitudinal slip in percent read respectively:

$$\begin{aligned}\alpha_{1,2} &= -\delta + \frac{x_4 + l_f x_2}{x_3}\frac{180}{\pi} \\ \alpha_{3,4} &= \frac{x_4 - l_r x_2}{x_3}\frac{180}{\pi}\end{aligned} \tag{32}$$

$$\begin{aligned}k_{1,2} &= -\left(1 - \frac{x_{10}}{x_3} R_f\right) \times 100 \\ k_{3,4} &= -\left(1 - \frac{x_8}{x_3} R_r\right) \times 100\end{aligned} \tag{33}$$

Finally, the axles forces are evaluated by adding together the tyre forces on each axle:

$$\begin{aligned}F_{fy} &= F_{y1} + F_{y2} \\ F_{fx} &= F_{x1} + F_{x2} \\ F_{ry} &= F_{y3} + F_{y4} \\ F_{rx} &= F_{x3} + F_{x4}\end{aligned} \tag{34}$$

In Section 6 we referred to the tyre saturation level as a measure for evaluating whether the vehicle is working more or less close to the limit of its performance envelope. We define the saturation level of the tyre either in longitudinal or lateral direction as follows. Let us consider a tyre generating the lateral force F_{yi} and the longitudinal force F_{xi} at the actual working conditions a_i, k_i, F_{zi} and γ_i. The lateral saturation is defined as the ratio between F_{yi} and the maximum lateral force obtainable while keeping k_i constant:

$$\begin{aligned}&F_{y\_MAX} = \max_{\alpha}\left(F_{y(combined)}\right) \quad \text{constant longitudinal slip } k_i, \alpha \text{ varying} \\ &Lat\_sat = \frac{F_{yi}}{F_{y\_MAX}} \times 100 \quad [\%]\end{aligned} \tag{35}$$

Similarly, for the longitudinal saturation we may write:

$$F_{x\_MAX} = \max_{k}\left(F_{x\,(combined)}\right) \quad \text{constant slip angle } \alpha_i, k \text{ varying}$$
$$Long\_sat = \frac{F_{xi}}{F_{x\_MAX}} \times 100 \quad [\%] \tag{36}$$

APPENDIX 2. TIME TO DISTANCE SCALING FACTOR

In this last section we shall derive the expression for the scaling factor S_{CF} of equation (5b), which is used to change the time derivatives in the vehicle equations of motion into derivatives with respect to the distance travelled along a defined path. Our formulation is a development of that employed by [1].

Referring to Figure 23, the relationship between the vehicle travelled distance ds_V and the time increment dt may be written as follows:

$$\frac{ds_V}{dt} = V = \sqrt{x_3^2 + x_4^2} \tag{37}$$

Then, the distance ds_V must be projected on the direction of the tangent to the path. In order to do this, we may write:

$$ds_1 = ds_V \cdot \cos\left(\nu - \psi_t\right) \tag{38}$$

A further condition has to be accounted for. If the vehicle is cornering, the distance that it has to travel depends on whether it takes an inner line or an outer line with respect to the ideal path. The relationship between the increment of the travelled distance in the direction of the tangent to the path ds_1 and the corresponding increment of the path length ds can be written as:

$$\frac{ds_1}{ds} = \frac{(r-d)}{r} = \left(1 - \frac{d}{r}\right) \tag{39}$$

Here, r is the corner radius and d is the distance of the vehicle centre of gravity from the ideal path. Knowing the position of the car in the absolute reference axis system fixed in space (x_6, x_5) and the co-ordinate (x_t, y_t) and the orientation ψ_t of the corresponding point on the ideal path (see Figure 2), the distance d may be calculated with the following expression:

$$d = \left(x_6 - y_t\right)\cos\left(\psi_t\right) - \left(x_5 - x_t\right)\sin\left(\psi_t\right) \tag{40}$$

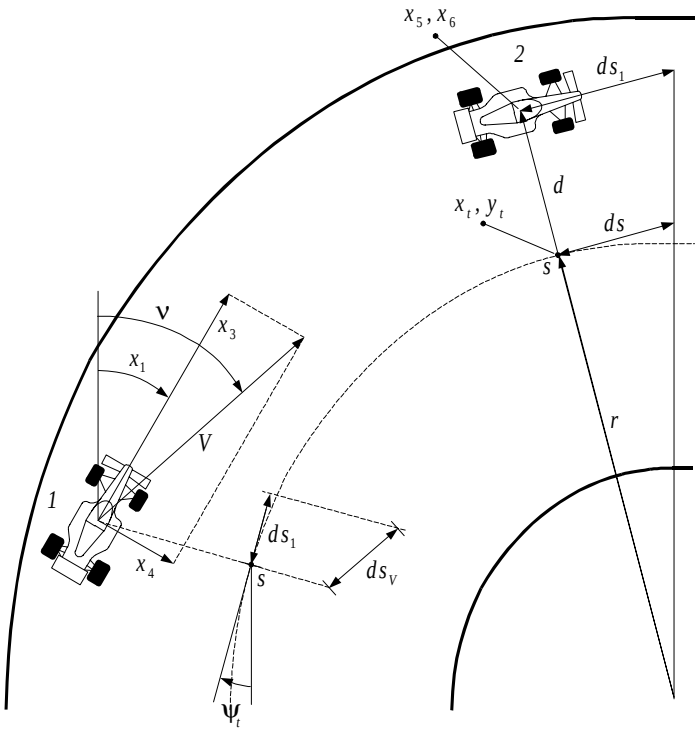

Fig. 23. Vehicle travelled distance projected onto the ideal path

The scaling factor required to determine the state derivatives in the new independent variable s can now be calculated:

$$\frac{d\mathbf{x}}{dt} = \frac{d\mathbf{x}}{ds} \cdot \frac{ds}{ds_1} \cdot \frac{ds_1}{ds_V} \cdot \frac{ds_V}{dt} = \frac{d\mathbf{x}}{ds} \cdot \frac{V \cdot \cos(\nu - \psi_t)}{(1 - d/r)} \tag{41}$$

Hence:

$$\frac{d\mathbf{x}}{ds} = \frac{d\mathbf{x}}{dt} \cdot \frac{(1 - d/r)}{\sqrt{x_3^2 + x_4^2} \cdot \cos(\nu - \psi_t)} = \frac{d\mathbf{x}}{dt} \cdot S_{CF} \tag{42}$$

By assuming that $x_4 << x_3$, the following approximations hold:

$$\nu = \arctan(x_4 / x_3) + x_1 \cong (x_4 / x_3) + x_1 \tag{43}$$

$$\sqrt{x_3^2 + x_4^2} \cong x_3 \tag{44}$$

By substituting equations (43) and (44) in equation (42) and doing some further manipulation, the final expression for the scaling factor reads:

$$S_{CF} = \frac{(1 - d / r)}{x_3 \cdot \cos(x_1 - \psi_t) - x_4 \cdot \sin(x_1 - \psi_t)} \tag{45}$$